Eur. Phys. J. B **34**, 351–357 (2003)
DOI: 10.1140/epjb/e2003-00231-3

THE EUROPEAN PHYSICAL JOURNAL B

Electric-field and magnetic-field effects on electronic tunneling through magnetic-barrier nanostructures

Maowang Lu[a], Zhenhong Dai, Lide Zhang, and Xiaohong Yan

Institute of Solid State Physics, Chinese Academy of Sciences, PO Box 1129, Hefei 230031, PR China

Received 23 July 2002 / Received in final form 20 May 2003
Published online 11 August 2003 –

Abstract. We have theoretically investigated electric-field and magnetic-field effects on electronic transport properties in nanostructures consisting of realistic magnetic barriers created by lithographic patterning of ferromagnetic or superconducting films. The results indicate that the characteristics of transmission resonance are determined not only by the magnetic configuration and the incident wave vector but also strongly by the applied electric and magnetic fields. It is shown that transmission resonance shifts towards the low-energy region by applying the electric field, and that with increasing the electric field transmission resonance is suppressed for the entire incident wave vector in the magnetic nanostructures with antisymmetric magnetic profile, while for the magnetic nanostructures with symmetric magnetic profile transmission resonance is enhanced for certain incident wave vector. It is also shown that both transmission and conductance shift towards high-energy direction and are greatly suppressed with the increase of the external magnetic field.

PACS. 73.40.Gk Tunneling – 73.23.-b Electronic transport in mesoscopic system – 75.70.Cn Interfacial magnetic properties (multilayers, superlattices)

1 Introduction

Electronic transport properties of magnetic-barrier nanostructures have attracted considerable attention owing to the advance in the microfabrication technique and potential applications to electronic devices in the recent years [1–16]. Present advances in nanofabrication allow one to produce this type of nanostructures, by the deposition of a heterostructure containing a high mobility two-dimensional electron gas (2DEG) in an inhomogeneous magnetic field, such as, microscopic magnetic barriers with amplitude of several thousand gauss have been formed in nonplanar devices [3] or by gating a 2DEG with micromagnets [4–6] or superconductors [7]. Experimentally, magnetoresistance oscillations *via* the commensurability effect between the classical cyclotron diameter and the period of a magnetic superlattice have been observed [4,5,7]. Very recently, a sharp resistance resonance effect has also been observed due to the formation of two types of magnetic edge states [11]. Theoretically, studies on electron tunneling through magnetic barriers [1,2,9] and magnetic superlattices [8] showed that the magnetic barriers possess wave-vector filtering, and magnetic minibands in the energy spectrum are formed in magnetic superlattice [8]. Quantum transport properties in magnetic superlattices under the influence of dc electric fields [12] and ac electric fields [13] have been explored. Very recently, effects of an applied electric field on electronic tunneling in rectangular-magnetic-barrier structures have been investigated [14]. However, the external magnetic-field effect on the tunneling transport properties of electrons in magnetic-barrier nanostructures remains unconsidered and the magnetic barriers used in reference [14] are not realistic ones. In this paper, we employ the realistic magnetic barriers instead of the ideal ones, and an electric field and a uniform magnetic field are further applied to these magnetic barriers. The noticeable wave-vector-dependent, electric-field-dependent, and magnetic-field-dependent tunneling features are revealed.

2 Model and method

We consider four realistic magnetic barriers [1] labeled by (a–d), which are formed, respectively, by the deposition, on top of a heterostructure, of a ferromagnetic stripe with magnetization (a) perpendicular and (b) parallel to the 2DEG, (c) of a conduction stripe with a current driven through it, and (d) of a superconducting plate interrupted by a stripe. For these four magnetic-barrier nanostructures, the magnetic fields (along the z direction) experienced by the 2DEG in the (x, y) plane are given by

$$\mathbf{B} = B(x, z_0)\hat{z},$$
$$B(x, z_0) = B_0[K(x + d/2, z_0) - K(x - d/2, z_0)], \quad (1)$$

[a] e-mail: mao-wang-lu@sohu.com

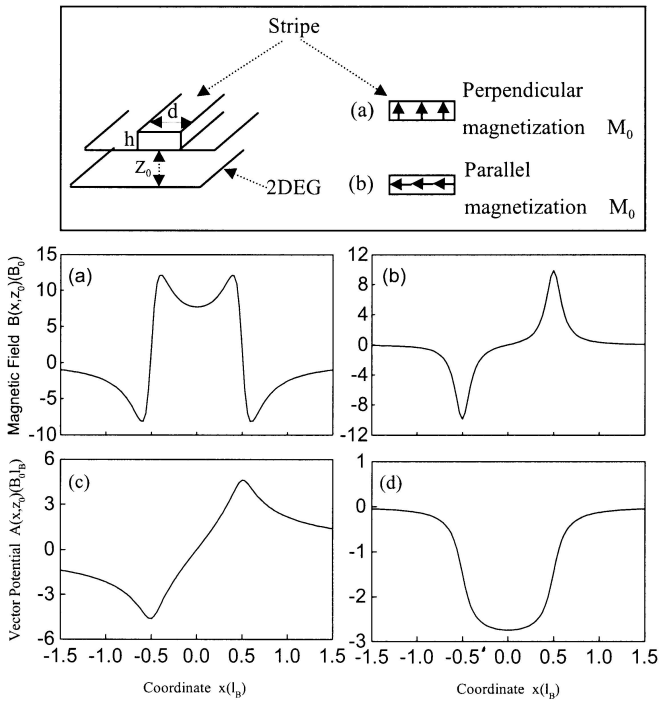

Fig. 1. Two realistic magnetic barriers (see (a) and (b)) and corresponding magnetic vector potentials (see (c) and (d)), where the schematic illustration of the system is placed on the top and the structural parameters are both chosen to be $d = 1$, and $z_0 = 0.1$.

where (a) $B_0 = M_0 h/d$, $K(x, z_0) = 2xd/(x^2 + z_0^2)$, (b) $B_0 = M_0 h/d$, $K(x, z_0) = -z_0 d/(x^2 + z_0^2)$, (c) $B_0 = I/d$, $K(x, z_0) = \ln[(x^2 + z_0^2)/d^2]$, and (d) $B(x, z_0) = B_0 \,\mathrm{Re}[1/\sqrt{1 - (x + iz_0)^2}]$. M_0, h, and d are the magnetization, height, and thickness of the stripes, I is the current driven through the stripe, and z_0 is the distance between the stripes and the 2DEG. According to these magnetic-field expressions, these four magnetic barriers can be classified into two groups: the symmetric magnetic barriers, $B(-x, z_0) = B(x, z_0)$, containing (a) and (d); and the antisymmetric magnetic barriers, $B(-x, z_0) = -B(x, z_0)$, having (b) and (c). Therefor, we only consider symmetric magnetic barrier (a) and antisymmetric one (b) for simplicity, however, our obtained results also can be extended the cases of magnetic barriers (c) and (d). Landau magnetic vector potentials $\mathbf{A}(x, z_0) = [0, A(x, z_0), 0]$ of magnetic barriers (a) and (b) are given by $A(x, z_0) = B_0 d \ln\{[(x + d/2)^2 + z_0^2]/[(x - d/2)^2 + z_0^2]\}$ and $A(x, z_0) = B_0 d\{\arctan[(x - d/2)/z_0] - \arctan[(x + d/2)/z_0]\}$, respectively. In Figure 1, we present these two magnetic barriers as well as their magnetic vector potentials and the schematic illustration of the system is also shown on its top, where the structural parameters are both chosen to be $d = 1.0$, $z_0 = 0.1$, the left and right ends of the barriers are assigned as $x_- = -1.5$ and $x_+ = 1.5$, respectively, and the magnetic field is in units of B_0.

The Hamiltonian for the 2DEG in the above magnetic-barrier nanostructures under an applied electric field $F\hat{x}$ (along the x direction) or an applied bias voltage $V_\alpha = F(x_+ - x_-)$ and an external uniform magnetic field $B_{ex}\hat{z}$ (along the z direction) is described by

$$H = \frac{1}{2m^*}[\mathbf{P} + e\mathbf{A}(x)]^2 - eFx, \tag{2}$$

where m^* is the effective mass of electron, $\mathbf{P}$ is the momentum of electron, and $A(x)$ is the total Landau magnetic vector potential consisting of $A(x, z_0)$ of the magnetic barrier and $A_{ex}(x) = B_{ex}[x - (x_+ + x_-)/2]$ of the external magnetic field. We express quantities in dimensionless units by using the cyclotron frequency $\omega_c = eB_0/m^*$ and the magnetic length $l_B = \sqrt{\hbar/eB_0}$. For GaAs, $m^* = 0.067m_e$ (m_e is the free-electron mass) and an typical magnetic field $B_0 = 0.2T$ [15], we obtain $l_B = 57.5$ nm and $\hbar\omega_c = 0.34$ meV. Since the problem described by equation (2) is translationally invariant along the y direction, the total wave function can be written as a product $\Psi(x, y) = \mathrm{e}^{iqy}\psi(x)$, where q is the wave vector in the y direction. Accordingly, we obtain the one-dimensional (1D) Schrödinger equation

$$\left\{\frac{d^2}{dx^2} - [A(x) + q]^2 + \frac{2eV_\alpha x}{(x_+ - x_-)} + 2E\right\}\psi(x) = 0, \tag{3}$$

where the function $U(x, q, V_\alpha, B_{ex}) = [A(x) + q]^2/2 - eV_\alpha x/(x_+ - x_-)$ is often interpreted as the $q-$dependent effective electric potential of the corresponding magnetic nanostructure, which depends on the magnetic configuration $B(x, z_0)$, the wave vector q, the applied bias voltage V_α or the external electric field F, and the external magnetic field B_{ex}. In the left and right regions, the wave functions can be written as $\psi(x) = \mathrm{e}^{ik_l x} + r\mathrm{e}^{-ik_l x}$, $x < x_-$, and $\psi(x) = t\mathrm{e}^{ik_r x}$, $x > x_+$, where $k_l = \sqrt{2E - q^2}$, $k_r = \sqrt{2(E + eV_\alpha) - q^2}$, and r and t are the reflection and transmission amplitudes, respectively. The effective potential $U(x, q, V_\alpha, B_{ex})$ in equation (3) is very complicated due to the magnetic profile $B(x, z_0)$ and its magnetic vector potential $A(x, z_0)$, and thus no exact schemes are available for solving the Schrödinger equation (3). Here, we use the method in reference [16] to solve equation (3), and the transmission coefficient through the magnetic-barrier nanostructure with an applied electric or magnetic field can be obtained by

$$T(E, q, V_\alpha, B_{ex}) = |t|^2. \tag{4}$$

With the transmission coefficient, at zero temperature we can calculate ballistic conductance at zero bias (*i.e.*, $V_\alpha = 0$)[1,2]

$$G(E_F, B_{ex}) = G_0 \int_{-\pi/2}^{\pi/2} T\left(E_F, \sqrt{2E_F}\sin\theta, 0, B_{ex}\right)\cos\theta d\theta, \tag{5}$$

where θ is the angle of incidence relative to the x direction, E_F is the Fermi energy, and $G_0 = e^2 m^* v_F L_y/\hbar^2$, where L_y is the length of the structure in the y directing and v_F the Fermi velocity.

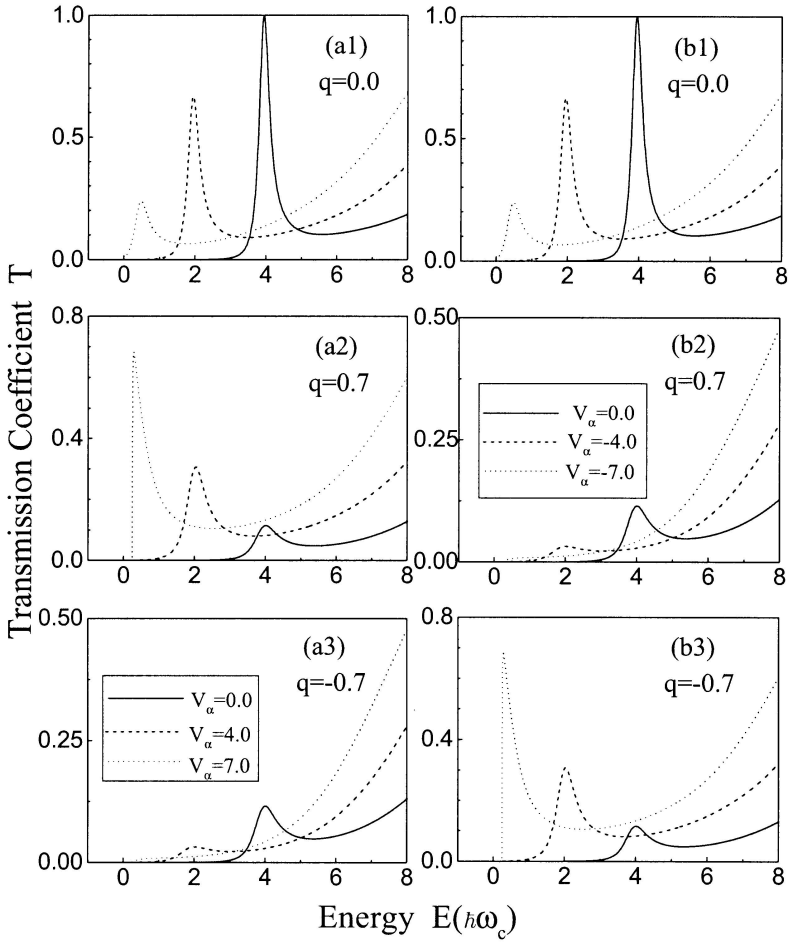

Fig. 2. Transmission coefficient for the magnetic barrier presented in Figure 1a under different applied biases V_α (in units of $\hbar\omega_c/e$), where the structural parameters are chosen to be $d = 1$, and $z_0 = 0.1$.

Under an applied bias V_α, the transmission current I of electrons through magnetic nanostructures can also be derived from the transmission coefficient T by

$$I(V_\alpha) = I_0 \int_0^\infty dE\sqrt{E}\left[f\left(E, E_F^{left}\right) - f\left(E, E_F^{right}\right)\right] \times \int_{-\pi/2}^{\pi/2} T\left(E, \sqrt{2E}\sin\theta, V_\alpha, 0\right)\cos\theta d\theta, \quad (6)$$

where $I_0 = L_y e\sqrt{m^*}/2\sqrt{2}\pi^2\hbar^2$, and $f\left(E, E_F^{left}\right)$ and $f\left(E, E_F^{right}\right)$ are the Fermi-Dirac distribution functions in the left and right electrodes, respectively. At zero temperature, equation (6) reduces to

$$I(V_\alpha) = I_0 \int_{E_0}^{E_F} dE\sqrt{E}\int_{-1}^{1} T(E, t, V_\alpha, 0)dt, \quad (7)$$

where $E_0 = (E_F - eV_\alpha)\Theta(E_F - eV_\alpha)$ and Θ is the Heaviside function.

3 Results and discussion

Figure 2 shows the transmission coefficient for electron tunneling through a single-barrier magnetic nanostructure presented in Figure 1a with and without applied biases, where the structural parameters are chosen to be $d = 1$, and $z_0 = 0.1$. Here and in the following, the bias voltage V_α is in units of $\hbar\omega_c/e$. At zero bias, one can clearly see from the solid curve in this figure that there is an obvious low-energy resonance peak in transmission spectrum due to the effective potential in equation (3) equivalent to a double-barrier electric potential for $|q|$ being small. Under a positive (see the left column a1–a3) or negative (see the right column b1–b3) applied bias, the characteristic of transmission resonance is greatly altered. For this magnetic-barrier nanostructure, its magnetic field profile and the corresponding magnetic vector potential are symmetric and antisymmetric, respectively, *i.e.*, $B(x, z_0) = B(-x, z_0)$ (see Fig. 1a) and $A(x, z_0) = -A(-x, z_0)$ (see Fig. 1c). Our calculated results show that cases under both positive bias and negative bias are the same for $q = 0$, and that for $q > 0$ the case of positive bias is the same as that of negative bias for $q < 0$; namely, electronic tunneling through this type of

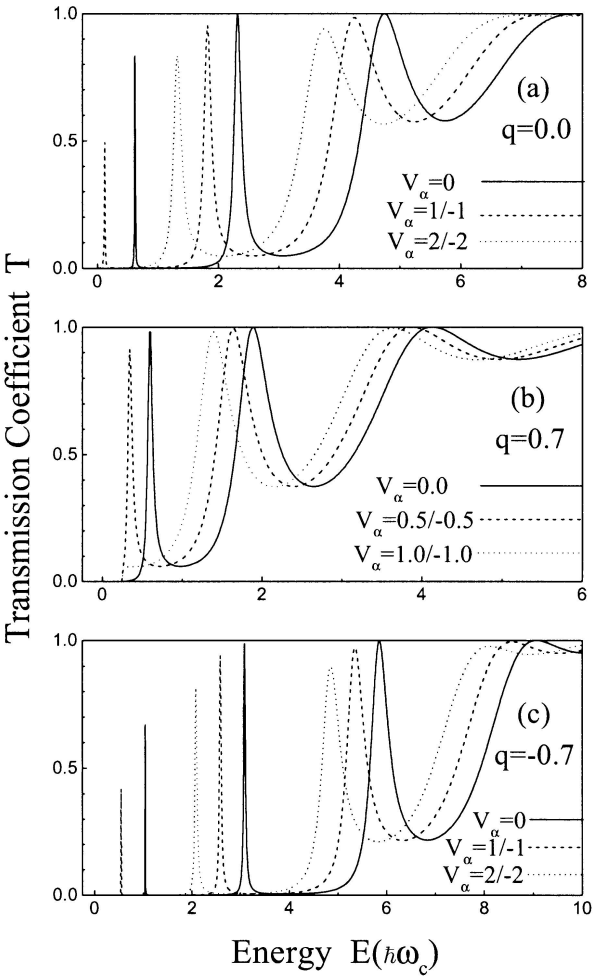

Fig. 3. Transmission coefficient for a nanostructure consisting of two magnetic barriers, in which a barrier shown in Figure 1b is followed by an identical one under different applied biases. The structural parameters still are chosen to be $d = 1$, and $z_0 = 0.1$.

magnetic-barrier nanostructure is symmetric about both the wave vector q and bias voltage V_α. When the applied positive or negative bias increases, one can see that the resonance peak shifts towards low-energy region for entire wave vector. However, the variation of amplitude of low-energy resonant peak with the applied biases depends strongly on wave vector q. For $q = 0$, the transmission resonance is suppressed under both increased positive and negative biases. For $q > 0$, transmission resonance is enhanced with increasing positive biases, while squashed under the increased negative biases. For $q < 0$, the changing cases in transmission resonance are the opposite as those for $q > 0$. Therefore, the external electric field strengthens the anisotropy of the transmission coefficient with wave vector q.

Figure 3 presents numerical results of transmission coefficient under positive and negative biases for electron tunneling through a double-barrier magnetic nanostructure consisting of two identical magnetic barriers, in which a magnetic barrier given in Figure 1b is followed by a identical one, and the parameters are chosen to be $d = 1$, and $z_0 = 0.1$. For this kind of magnetic barrier with antisymmetric magnetic profile $B(x, z_0) = -B(-x, z_0)$ and symmetric vector potential $A(x, z_0) = A(-x, z_0)$ (see Figs. 1b and 1d, respectively), we see from Figure 3 that the cases are the same for positive bias and negative bias when $B_{ex} = 0$. Here it should be noted that the direction of the electric field $\mathbf{F}$ and the applied bias V_α are opposite to each other, *i.e.*, for negative bias, the direction of electric field is from left to right. In contrast to the case for electron tunneling through the magnetic nanostructure containing one barrier with the symmetric magnetic profile shown in Figure 1a, one can easily see that the transmission spectrum exhibits more, sharper, and more complex resonance peaks in low-energy regions. Moreover, when the positive bias or negative bias increases, the transmission resonance peaks shift towards lower energy regions and are suppressed for entire wave vector q range. These features are different from those for single-barrier nanostructure due to their different magnetic configurations.

In Figure 4 we show the transmission current I for electron with different Fermi energy tunneling through single-barrier magnetic nanostructure presented in Figure 1a (see the left column (a1–a3)) and double-barrier one given in Figure 1b (see the right column (b1–b3)), where the structural configurations and parameters are the same as in Figure 2 and in Figure 3 for the single-barrier and double-barrier nanostructures, respectively. It is well-known that for a 2DEG the Fermi energy can be derived by $E_F = (\hbar^2\pi/m^*)n_e$, where $\hbar$ is the reduced Plank constant, and m^* and n_e are the effective mass and number density of electrons, respectively. Therefore, for the GaAs material the Fermi energy of the 2DEG is completely determined by the electron number density n_e, and thus in the conventional $GaAs/Ga_{0.7}Al_{0.3}As$ heterostructure with [11] $n_e \sim 10^{15}$ m^{-2} the $E_F = 3.55$ meV $\approx 10(\hbar\omega_c)$. However, here we take several Fermi energy values to demonstrate the effect of n_e on transmission current through the magnetic-barrier nanostructures under the applied bias. Despite the averaging of transmission coefficient (see Eq. (7)), the resonance features similar to the transmission coefficient under applied biases are also reflected in $I - V_\alpha$ characteristic of tunneling magnetic-barrier nanostructures, especially for the small E_F (see Figs. 4a1 and 4b1). Moreover, it can be seen from Figures 4a1–4a3 that there exists a slight discrepancy between the positive bias and the negative bias for single-barrier magnetic nanostructure for the sake of transmission coefficient T, but they are the same (see Figs. 4b1–4b3) for the double-barrier magnetic nanostructure due to the symmetry of transmission coefficient about the bias V_α as shown in Figure 3. One can also see that the $I - V_\alpha$ characteristic exhibits an obvious negative-differential-conductivity (NDC) effect for both magnetic-barrier nanostructures, and this effect shows a strong E_F-dependence. When the Fermi energy or the number density of the 2DEG decreases the degree of the NDC effect becomes weak even disappears, which also implies

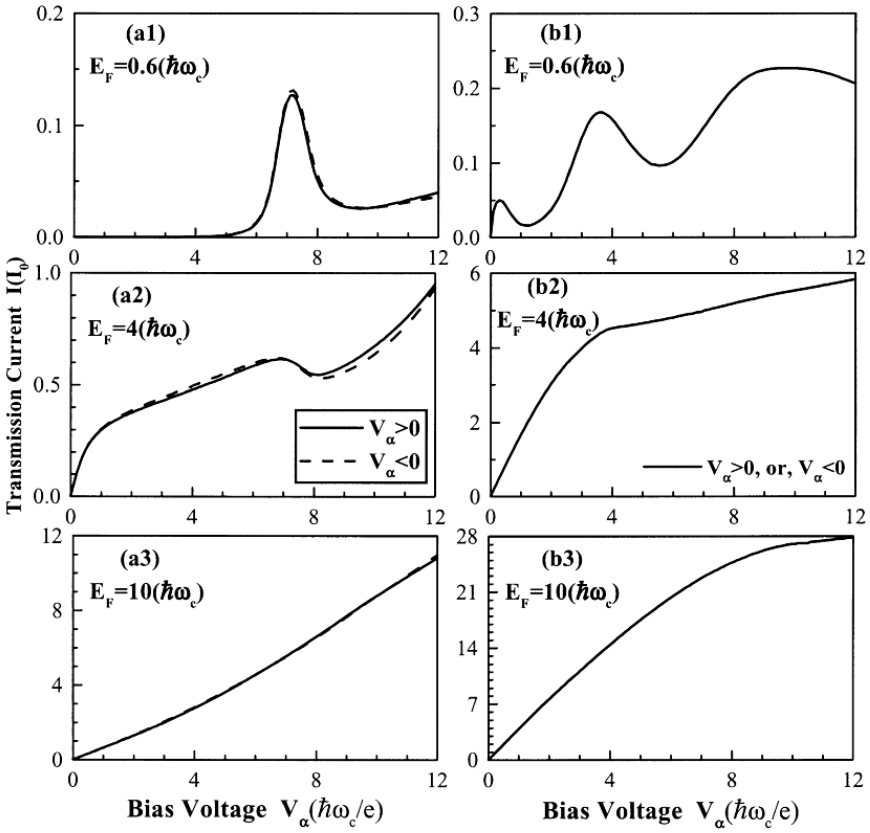

Fig. 4. Transmission current through magnetic barriers for different Fermi energy E_F. (a1–a3) A single-barrier nanostructure, where the parameters are the same as in Figure 2. (b1–b3) A double-barrier nanostructure, where the structural configuration and its parameters are the same as in Figure 3.

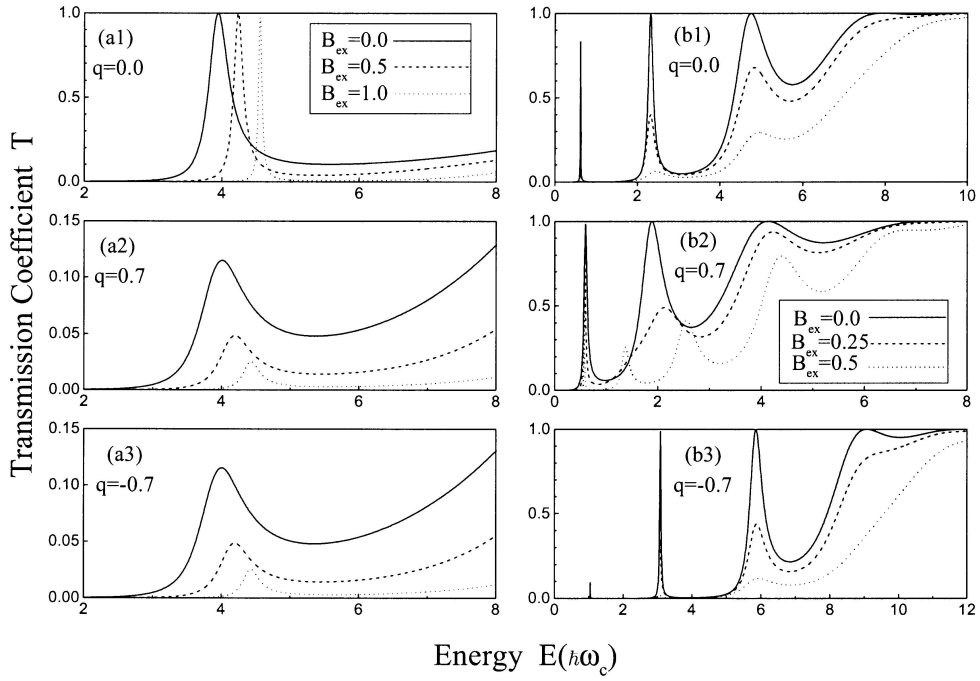

Fig. 5. Transmission coefficient for magnetic-barrier nanostructures under different magnetic field. The left column (a1–a3) is for single barrier, while the right column (b1–b3) is for double barrier, and structural configurations and parameters are the same as in Figure 4.

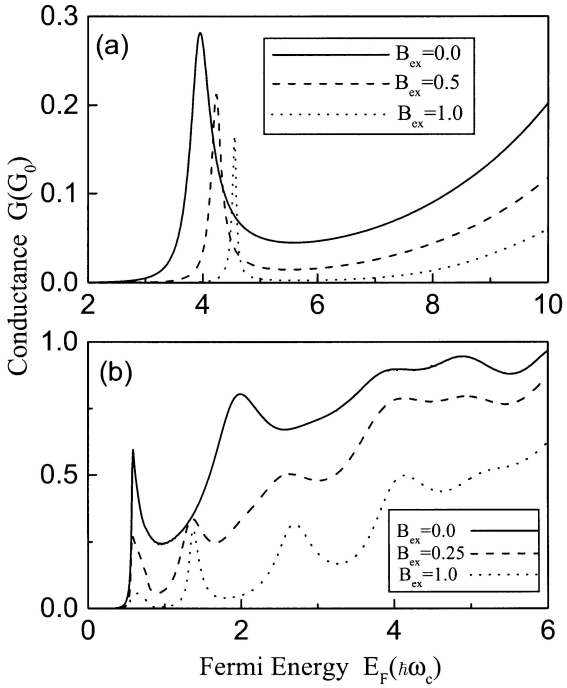

Fig. 6. Conductance through magnetic-barrier nanostructures under different magnetic fields. (a) and (b) correspond to the single-barrier and double-barrier nanostructures, respectively, where structural parameters and configurations are the same as in Figure 4.

that adjusting the n_e can improve the NDC properties of magnetic-barrier nanostructures.

Figure 5 presents the transmission coefficient for an electron tunneling through two magnetic-barrier nanostructures under different applied magnetic fields. The left column (a1–a3) corresponds to the single-barrier nanostructure as shown in Figure 1a, where the structural parameters are the same as in Figure 2. The right column (b1–b3) is for the double-barrier nanostructure with the same structural parameters and configuration as in Figure 3. The external magnetic field $\mathbf{B}_{ex}$ along the z direction is in units of B_0 and is assumed not to influence the original magnetic profile here. For the single-barrier magnetic nanostructure one can see from Figures 5a2 and 5a3 that the case for $q > 0$ is completely the same as that for $q < 0$. As an external magnetic field is applied, the transmission resonance is greatly altered for electron tunneling through these two magnetic nanostructures. Moreover, with the external magnetic field increasing, the transmission resonance through both magnetic nanostructures shifts towards high-energy region (which is just the opposite to that for electric field case) and is greatly suppressed for entire wave vector range.

Finally, we study the conductance through magnetic-barrier nanostructures under the influence of an applied magnetic field. Figure 6a shows the conductance through single-barrier nanostructures given in Figure 1a, where the parameters are chosen to be the same as in Figure 2, and the solid, dashed, and dotted curves correspond to the external field $B_{ex} = 0$, 0.5, and 1.0, respectively. Despite the averaging of $T(E, q, 0, B_{ex})$ over half the Fermi surface, the main features of the electron transmission is still reflected at conductance. From Figure 6a one sees that at zero magnetic field the conductance has a resonant peak in the low Fermi energy region. With B_{ex} increasing, the resonant peak shifts towards high Fermi energy and is squashed. In Figure 6b we present the conductance through a nanostructure consisting of two identical magnetic barriers under an external magnetic field. Here $B_{ex} = 0$, 0.25, and 0.5 correspond to the solid, dashed, and dotted curves, respectively. The conductance has also a resonance structure, and its main feature is similar to that of Figure 6a. Moreover, the resonant peaks are greatly suppressed as the applied magnetic field increases.

Here, we would like to point out that since we calculate the conductance and the transmission current from the equations (5) and (7), respectively, all the results presented so far are obtained at zero temperature and in the ballistic regime. In the present work, we consider ballistic transport of high mobility two-dimensional electron gases (2DEG) with the mean free path not less than the dimension of magnetic-barrier nanostructures in tunneling direction. For the finite temperature effect on electronic tunneling through magnetic-barrier nanostructures, it is known that at a finite temperature T the main contribution to both the ballistic conductance and the transmission current comes from electrons with energy located in the region $(E_F - k_BT, E_F + k_BT)$. Therefore, at a finite temperature our results may survive if the effective potential $U(x, q, V_a, B_{ex})$ of magnetic nanostructure is taken to be $U(x, q, V_a, B_{ex}) \gg k_BT$ by means of adjusting the structural parameters and the applied external electric or magnetic field, because in this case resonant tunneling is still the dominant transport mechanism.

4 Conclusions

In summary, we have studied the electronic tunneling transport properties in the realistic magnetic-barrier nanostructures under the influence of both an applied electric field and an uniform magnetic field. Features of tunneling properties through these magnetic-barrier nanostructures depend not only on the configurations and the incident wave-vector, but also strongly on the applied electric field as well as the external magnetic field. The transmission resonance shifts towards low-energy region for entire incident wave-vector when an applied electric field increases. For the magnetic barriers with antisymmetric magnetic field the transmission resonance is drastically suppressed with increasing the electric field, while for magnetic barriers with symmetric magnetic field the transmission resonance is enhanced for certain incident wave-vectors under an applied electric field. As an external magnetic field increases, both transmission resonance and conductance shift towards high-energy region and is successively squashed. The $I - V$ characteristic exhibits obvious negative-differential conductivity for electron tunneling through the magnetic-barrier nanostructures.

This work was supported by National Major project of Fundamental Research of China: nanometerials & nanostructures and by the National Natural Science Foundation of China under Grant No. 10074064.

References

1. A. Matulis, F.M. Peeters, P. Vasilopoulos, Phys. Rev. Lett. **72**, 1518 (1994)
2. J.Q. You, Lide Zhang, P.K. Ghosh, Phys. Rev. B **52**, 17243 (1995)
3. M.L. Leadbeater, C.L. Foden, J.H. Burroughes, M. Pepper, T.M. Burke, L.L. Wang, M.P. Grimshaw, D.A. Ritchie, Phys. Rev. B **52**, R8629 (1995)
4. P.D. Ye, D. Weiss, R.R. Gerhardts, M. Seeger, K. von Klitzing, K. Eberl, H. Nickel, Phys. Rev. Lett. **74**, 3013 (1995)
5. M. Kato, A. Endo, S. Katsumoto, Y. Iye, Phys. Rev. B **58**, 4876 (1998)
6. V. Kubrak, F. Rahman, B.L. Gallagher, P.C. Main, M. Henini, C.H. Marrows, M.A. Howson, Appl. Phys. Lett. **74**, 2507 (1999); F.M. Peeters, X.Q. Li, *ibid.* **72**, 572 (1998)
7. H.A. Carmona, A.K. Geim, A. Nogaret, P.C. Main, T. Foster, M. Henini, S.P. Beaumont, M.G. Blamire, Phys. Rev. Lett. **74**, 3009 (1995)
8. I.S. Ibrahim, F.M. Peeters, Phys. Rev. B **52**, 17321 (1995); A. Krakovsky, *ibid.* B **53**, 8469 (1996); Z.Y. Zeng, L.D. Zhang, X.H. Yan, J.Q. You, Phys. Rev. B **60**, 1515 (1999)
9. Y. Guo, B.L. Gu, Z.Q. Li, Q. Sun, Y. Kawazoe, Eur. Phys. J. B **3**, 257 (1998); *ibid.* **3**, 263 (1998)
10. A. Matulis, F.M. Peeters, Phys, Rev. B **62**, 91 (2000)
11. A. Nogaret, S.J. Bending, M. Henini, Phys. Rev. Lett. **84**, 2231 (2000)
12. Y.M. Mu, Y. Fu, M. Willander, Superlattices Microstruct. **22**, 135 (1997)
13. O.M. Yevtushenko, K. Richter, Phys. Rev. B **57**, 14839 (1998)
14. Y. Guo, H. Wang, B.L. Gu, Y. Kawazoe, Phys. Rev. B **61**, 1728 (2000)
15. G. Papp, F.M. Peeters, Appl. Phys. Lett. **78**, 2184 (2001); *ibid*, 79, 3198 (2001)
16. M.W. Lu, L.D. Zhang, Y.X. Jin, X.H. Yan, Eur. Phys. J. B **27**, 565 (2002)